 Related Commentary, page 3208

Smad4 loss in mice causes spontaneous head and neck cancer with increased genomic instability and inflammation

Sophia Bornstein,[1] Ruth White,[1,2] Stephen Malkoski,[3] Masako Oka,[2] Gangwen Han,[2] Timothy Cleaver,[3] Douglas Reh,[1] Peter Andersen,[1] Neil Gross,[1] Susan Olson,[4] Chuxia Deng,[5] Shi-Long Lu,[6] and Xiao-Jing Wang[1,2]

[1]Department of Otolaryngology, Oregon Health & Science University (OHSU), Portland, Oregon, USA. [2]Department of Pathology and [3]Department of Medicine, Division of Pulmonary Sciences and Critical Care Medicine, University of Colorado Denver, Aurora, Colorado, USA. [4]Department of Molecular and Medical Genetics, OHSU, Portland, Oregon, USA. [5]Genetics of Development and Disease Branch, NIDDK, NIH, Bethesda, Maryland, USA. [6]Department of Otolaryngology, University of Colorado Denver, Aurora, Colorado, USA.

Smad4 is a central mediator of TGF-β signaling, and its expression is downregulated or lost at the malignant stage in several cancer types. In this study, we found that Smad4 was frequently downregulated not only in human head and neck squamous cell carcinoma (HNSCC) malignant lesions, but also in grossly normal adjacent buccal mucosa. To gain insight into the importance of this observation, we generated mice in which *Smad4* was deleted in head and neck epithelia (referred to herein as *HN-Smad4*$^{-/-}$ mice) and found that they developed spontaneous HNSCC. Interestingly, both normal head and neck tissue and HNSCC from *HN-Smad4*$^{-/-}$ mice exhibited increased genomic instability, which correlated with downregulated expression and function of genes encoding proteins in the Fanconi anemia/Brca (Fanc/Brca) DNA repair pathway linked to HNSCC susceptibility in humans. Consistent with this, further analysis revealed a correlation between downregulation of Smad4 protein and downregulation of the Brca1 and Rad51 proteins in human HNSCC. In addition to the above changes in tumor epithelia, both normal head and neck tissue and HNSCC from *HN-Smad4*$^{-/-}$ mice exhibited severe inflammation, which was associated with increased expression of TGF-β1 and activated Smad3. We present what we believe to be the first single gene–knockout model for HNSCC, in which both HNSCC formation and invasion occurred as a result of Smad4 deletion. Our results reveal an intriguing connection between Smad4 and the Fanc/Brca pathway and highlight the impact of epithelial Smad4 loss on inflammation.

Introduction

Head and neck squamous cell carcinoma (HNSCC) is the sixth most common cancer worldwide (1). Despite recent advances in cancer biology and therapy, the 5-year survival for patients with HNSCC has remained 50% for the past 20 years (2). Several genetic alterations in HNSCC have been reported, including loss of genetic material on 9p (encoding p16), 17p (encoding *p53*) (1), 18q (encoding *DCC*, *Smad4*, and *Smad2*) (3–5), and the type II TGF-β receptor (*TGFBR2*) (6). Several oncogenic signaling pathways are also upregulated in HNSCC, including Ras, EGFR/Stat3, and PI3K/PTEN/Akt pathways (1, 7). Among them, Ras activation plays a role in HNSCC initiation but is insufficient for malignant conversion (8, 9). In contrast, loss of TGFβR2 is insufficient to initiate HNSCC formation but is a potent promoter in HNSCC tumorigenesis (8). In general, little is known about which somatic changes in HNSCC lesions play a causal role. To date, the best-studied germline mutations that lead to increased susceptibility to HNSCC are in genes belonging to the Fanconi anemia/Brca (Fanc/Brca) pathway (10).

Smad4 was originally identified as a tumor suppressor in pancreatic cancer (11) and subsequently characterized as a key mediator of TGF-β signaling (12). Termed the "common Smad," Smad4 plays an instrumental role in TGF-β/BMP signaling by forming complexes with receptor-activated Smads, i.e., Smad-2 and -3, or Smad-1 and -5. The Smad complexes then translocate to the nucleus to regulate gene expression of Smad targets involved in a wide variety of cancer-related processes including proliferation, apoptosis, and inflammation (13). Somatic inactivation of *Smad4* is a frequent event in multiple tumor types (14). *Smad4* deletion in murine tissues, in combination with other genetic alterations that cause tumor initiation, resulted in cancer lesions of the colon (15, 16), pancreas (17, 18), forestomach (19), and liver (20). Thus, Smad4 loss appears to play an important role in malignant progression. However, *Smad4* deletion in mice also resulted in spontaneous cancer formation of the stomach (21), skin (22–24), and mammary gland (23), suggesting that Smad4 loss has both initiation and promotion effects on tumorigenesis in these tissues. Other than that they cause loss of expression of TGF-β target genes associated with growth inhibition, little is known about the molecular mechanisms underlying Smad4 loss–associated tumorigenesis.

With respect to the role of Smad4 in HNSCC, the region on chromosome 18q where *Smad4* is located is frequently lost at the genetic level in HNSCC (25), and loss of heterozygosity (LOH) at the *Smad4* locus has been reported at approximately 50% (3, 4). Additionally, loss of the Smad4 protein is common in HNSCC, and this was correlated with depth of invasion and pathologic stage (26) as well as regional metastases and decreased survival (27). However, it is unknown at which stage Smad4 is downregulated in human HNSCC and whether Smad4 loss plays a causal role in HNSCC development and progression. To address these questions, we examined Smad4 levels in both grossly normal mucosa adjacent to HNSCC and neoplastic lesions of HNSCC patients. Unlike TGFβR2,

Conflict of interest: The authors have declared that no conflict of interest exists.
Citation for this article: *J. Clin. Invest.* **119**:3408–3419 (2009). doi:10.1172/JCI38854.

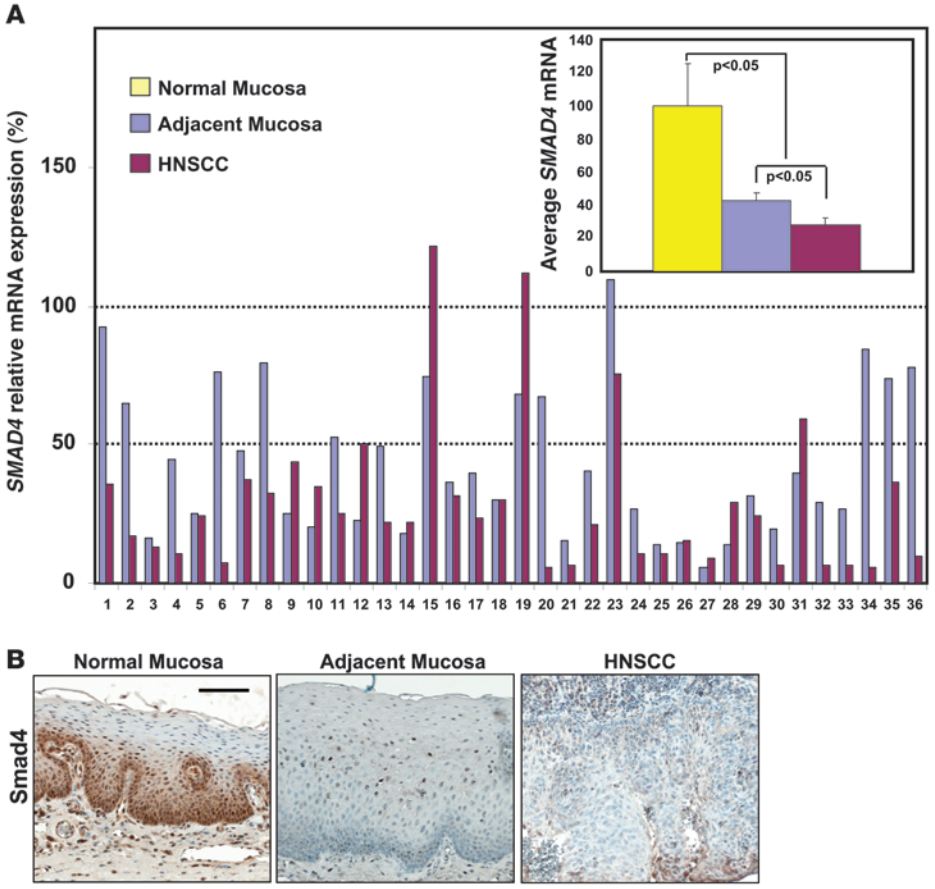

Figure 1
Smad4 downregulation is common in human HNSCC. (**A**) *SMAD4* mRNA expression examined by qRT-PCR of 7 normal sleep apnea control samples, 36 HNSCC samples, and 36 matched adjacent mucosa samples. The relative expression of *SMAD4* in sleep apnea controls was arbitrarily set as 100%. *SMAD4* downregulation was defined as less than 50% that of normal sleep apnea controls. The average *SMAD4* expression from each group is presented in the inset. Error bars indicate SEM, and significance was determined using Student's *t* test. (**B**) Smad4 IHC staining (brown). Thirty-six samples per group were stained, and a representative image is presented showing Smad4 protein loss in an HNSCC and matched adjacent mucosa compared with a normal sleep apnea control sample. Scale bar: 40 μm (all panels).

which was downregulated only in malignant HNSCC, Smad4 was downregulated in both grossly normal mucosa and malignant HNSCC lesions compared with normal head and neck tissues. We deleted *Smad4* specifically in murine head and neck epithelia and found that *Smad4*-knockout mice developed spontaneous HNSCC with evidence of increased genomic instability and inflammation.

Results

Smad4 downregulation occurred at an early stage in human HNSCC. To determine which stage Smad4 was downregulated in human HNSCC, we analyzed *SMAD4* mRNA levels in 36 pairs of human HNSCC and mucosa samples adjacent to each HNSCC by quantitative RT-PCR (qRT-PCR), using normal mucosa samples from sleep apnea patients as controls. Among these samples, 86% (31 of 36) of HNSCC samples exhibited downregulation of *SMAD4* mRNA to less than 50% of Smad4 levels in control mucosa samples. In addition, 67% (24 of 36) of adjacent mucosa samples exhibited more than 50% downregulation of Smad4, indicating that Smad4 loss occurred early in cancer development (Figure 1A). We then performed Smad4 immunohistochemistry (IHC) on these samples and found that overall, Smad4 protein staining patterns correlated with their mRNA levels, i.e., while Smad4 stained strongly in the normal control group, Smad4 staining was significantly reduced or lost in adjacent mucosa samples and HNSCCs (Figure 1B). To determine whether Smad4 reduction was due in part to genetic loss, we performed an LOH analysis using HNSCC samples that lost *SMAD4* mRNA, with paired adjacent mucosa samples as controls, and found that 33% (6 of 18) of sample pairs exhibited LOH at the *Smad4* locus (Supplemental Figure 1; supplemental material available online with this article; doi:10.1172/JCI38854DS1).

Deletion of Smad4 in murine head and neck epithelia resulted in spontaneous HNSCC that mimicked human HNSCC. The high frequency of Smad4 downregulation in human HNSCC, particularly at the stage prior to tumor formation, prompted us to investigate whether Smad4 loss played a causal role in HNSCC tumorigenesis. We used our inducible head and neck–specific knockout system (8, 9), which allows *Smad4* deletion (*HN-Smad4*$^{-/-}$) in head and neck epithelial cells upon RU486 application to the oral cavity (Supplemental Figure 2). We induced *Smad4* deletion in murine head and neck epithelia at 4 weeks of age. In total, 35 *HN-Smad4*$^{-/-}$, 9 *HN-Smad4*$^{+/-}$, and 23 *HN-Smad4*$^{+/+}$ mice (all on the C57BL/6 background) were monitored for tumor formation for up to 80 weeks. Beginning at 29 weeks of age, *HN-Smad4*$^{-/-}$ mice began to develop oral tumors. By 80 weeks, 74% (26 of 35) developed spontaneous oral tumors, and 12% (3 of 26) of tumor-bearing mice harbored regional lymph node metastases prior to being euthanized. Most tumor-bearing mice required euthanasia prior to the development of metastatic disease, due to difficulties with food intake or excessive bleeding, which are problems often encountered in human HNSCC patients. No tumors were observed in either *HN-Smad4*$^{+/-}$ or *HN-Smad4*$^{+/+}$ mice (Figure 2A).

Tumors generated in *HN-Smad4*$^{-/-}$ mice were derived from the buccal mucosa (Figure 2B) and palate (data not shown). Histologically, *HN-Smad4*$^{-/-}$ HNSCCs exhibited regions ranging from moderately to poorly differentiated squamous cell carcinoma (SCC).

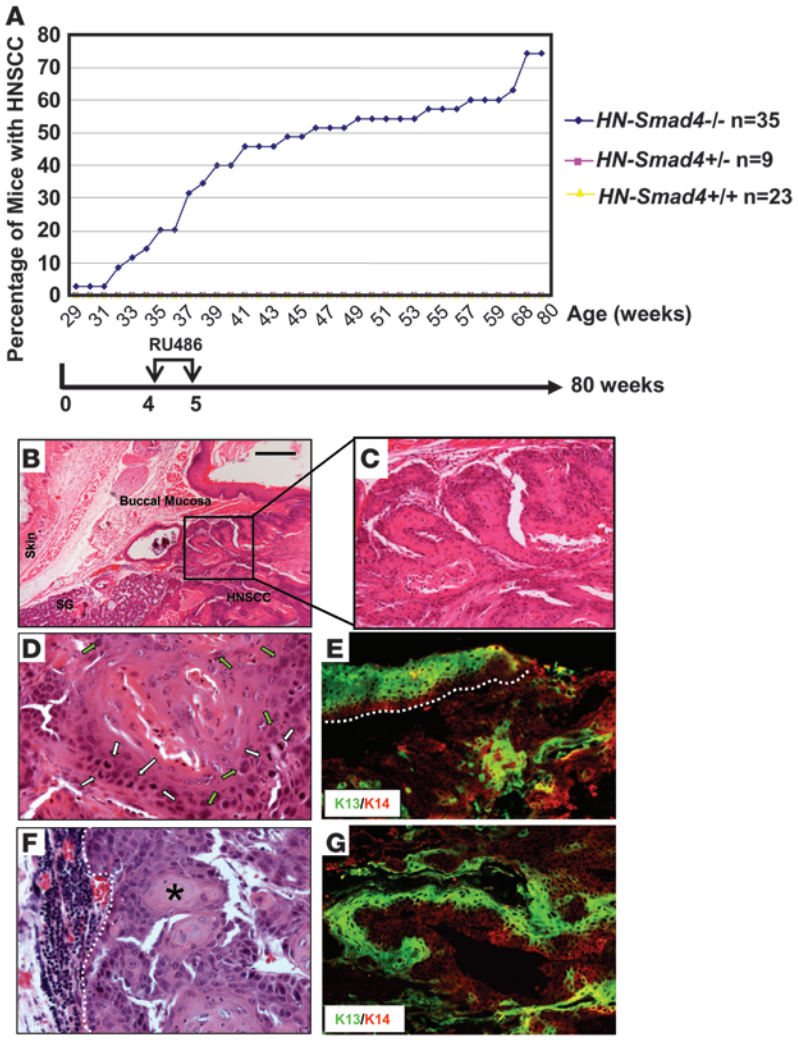

Figure 2
Spontaneous HNSCC in *HN-Smad4*$^{-/-}$ mice. (**A**) Kinetics of tumor formation. Tumor formation was assessed by biweekly examination of the oral cavity in live mice and necropsy at the time of euthanasia. Data points represent the percentage of tumor-bearing mice relative to the total number of mice in each group. (**B**) An H&E-stained tumor section of a buccal SCC in an *HN-Smad4*$^{-/-}$ mouse demonstrates that HNSCCs were derived from the buccal mucosa and not the skin of *HN-Smad4*$^{-/-}$ mice. SG, salivary gland adjacent to the HNSCC. (**C**) A dysplastic region in the HNSCC from **B**. (**D**) High magnification shows SCC cells with enlarged nuclei (green arrows) and increased mitosis (white arrows), indicative of malignant pathology. (**E**) Staining of K13 (green), which stains stratified epithelia, counterstained with the general keratinocyte marker K14 (red) in a buccal SCC from an *HN-Smad4*$^{-/-}$ mouse indicates tumors are derived from buccal mucosa. The white dotted line highlights the adjacent mucosa. (**F**) H&E tumor section of a lymph node metastasis in an *HN-Smad4*$^{-/-}$ mouse. The white dotted line delineates the boundary between metastatic tumor cells and lymph node tissue. The asterisk indicates a keratin pearl. (**G**) Staining of K13 (green), counterstained with K14 (red) in a lymph node metastasis from an *HN-Smad4*$^{-/-}$ mouse indicates the tumor is derived from an HNSCC. Scale bar: 100 μm (**B**); 40 μm (**C**, **E**, and **G**); 20 μm (**D** and **F**).

The precursor lesions displayed histology ranging from hyperplasia to dysplasia (Figure 2C), which is reflective of the histological stages seen during human head and neck cancer development. HNSCC cells displayed enlarged nuclei and increased mitoses (Figure 2D). Keratin staining revealed that the adjacent buccal mucosa of *HN-Smad4*$^{-/-}$ HNSCCs expressed keratin 13 (K13), which is a marker of oral epithelia (28), not hyperplastic epidermis, verifying that the tumors were derived from the oral cavity rather than the skin (Figure 2E). However, *HN-Smad4*$^{-/-}$ HNSCCs exhibited patchy loss of this differentiation marker, which is associated with malignant conversion (Figure 2E) (8). Histological sections of enlarged regional lymph nodes demonstrated HNSCC metastases. As shown in Figure 2F, keratin pearls, which are pathognomonic for SCCs, are adjacent to lymphatic tissue. Keratin staining of these lymph nodes (Figure 2G) further verified that metastases arose from HNSCC, as K13, as well as the general keratinocyte marker K14, both stained the lymph node section.

As a central mediator of TGF-β signaling, Smad4 mediates the well-documented tumor suppressor roles of TGF-β, such as growth inhibition and apoptosis, which are reflected in *HN-Smad4*$^{-/-}$ mucosa and HNSCC. Proliferating cell nuclear antigen (PCNA) staining for proliferative cells and TUNEL staining for apoptotic cells revealed increased cell proliferation and reduced apoptosis in *HN-Smad4*$^{-/-}$ mucosa and HNSCC compared with *HN-Smad4*$^{+/+}$ mucosa (Supplemental Figure 3). However, these changes did not explain why *Smad4* gene deletion alone was sufficient for HNSCC formation, as similar alterations were also observed in *Tgfbr2*$^{-/-}$ head and neck keratinocytes, which required additional Ras activation for HNSCC tumorigenesis (8). To determine whether loss of Smad4 facilitated Ras activation, we sequenced *KRAS* and *HRAS* genes in *HN-Smad4*$^{-/-}$ HNSCCs. From a total of 18 tumors examined, 4 exhibited *HRAS* mutations at codon 61. Among the tumors with *HRAS* mutations, 2 changed CAA to CTA, 1 changed CAA to CAC, and 1 changed CAA to CGA (Supplemental Figure 4A). All of these mutations are associated with *HRAS* activation (29). No *KRAS* mutation was detected in *HN-Smad4*$^{-/-}$ HNSCCs. While the minority of HNSCCs exhibited *Ras* mutation, similar to our previous observation in human HNSCC, tumors without a *Ras* mutation exhibited increased Ras protein levels (Supplemental Figure 4B). These data suggest that spontaneous Ras activation via mutation or overexpression could provide an initiation event for HNSCC formation in at least a subset of *HN-Smad4*$^{-/-}$ tumors. To test this, we generated mice with heterozygous deletion of *Smad4* together with heterozygous *HN-K-ras*^{G12D} mutation in the head and neck epithelia (*HN-K-ras*^{G12D}*Smad4*$^{+/-}$) using a breeding strategy similar to that in our previous report (8). *HN-K-ras*^{G12D}*Smad4*$^{+/-}$ mice devel-

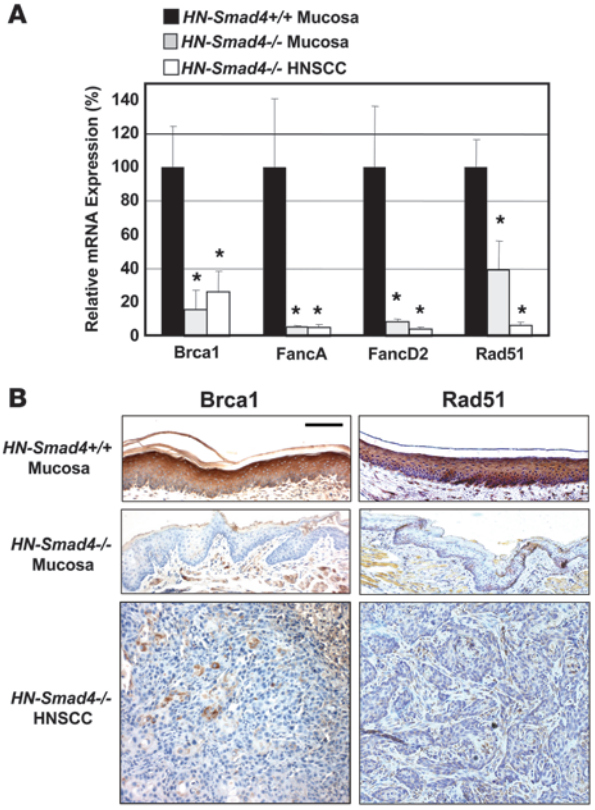

Figure 3
Downregulation of Fanc/Brca transcripts in *HN-Smad4*$^{-/-}$ mucosa and HNSCC. (**A**) Decreased relative mRNA expression of Brca1, FancA, FancD2, and Rad51 in *HN-Smad4*$^{-/-}$ mucosa and HNSCC, compared with *HN-Smad4*$^{+/+}$ mucosa by qRT-PCR. Means of 5–10 samples from each group are presented, and error bars indicate SEM. The average expression of Smad4 in the *HN-Smad4*$^{+/+}$ samples was arbitrarily set at 100%. **P* < 0.05 versus *HN-Smad4*$^{+/+}$ mucosa. (**B**) Decreased Brca1 and Rad51 protein by IHC in *HN-Smad4*$^{-/-}$ mucosa and HNSCC compared with *HN-Smad4*$^{+/+}$ mucosa. Five to 10 samples per group were analyzed, and a representative image is presented. Scale bar: 40 μm (all panels).

oped HNSCC within only 3 months of gene mutation/deletion (Supplemental Figure 4C). This result not only further confirmed that spontaneous Ras activation could provide an initiation event, but also suggests a haploid insufficiency of Smad4 in the setting of other initiating alterations in head and neck epithelia.

Downregulation of molecules in the Fanc/Brca pathway correlated with abnormal centrosomes and increased genomic aberrations in HN-Smad4$^{-/-}$ *HNSCC.* Invasive and metastatic HNSCC formation as well as spontaneous Ras mutation, resulting from Smad4 single-gene deletion, prompted us to assess whether DNA repair mechanisms resulting in genomic instability were perturbed after Smad4 loss. Among them, we found that expression levels of genes in the Fanc/Brca pathway were significantly altered after Smad4 deletion. Compared with *HN-Smad4*$^{+/+}$ mucosa, *HN-Smad4*$^{-/-}$ HNSCCs exhibited decreased mRNA expression of Brca1 by 74%, FancA by 95%, FancD2 by 96%, and Rad51 by 93%. In addition, *HN-Smad4*$^{-/-}$ mucosa exhibited reduced expression of Brca1 by 84%, FancA by 94%, FancD2 by 91%, and Rad51 by 61%, suggesting that these alterations occurred as a result of Smad4 deletion, prior to tumor formation (Figure 3A). The transcriptional downregulation of Brca1 and Rad51 in *HN-Smad4*$^{-/-}$ mucosa and HNSCC also correlated with their protein loss as detected by IHC (Figure 3B).

As defects in the Fanc/Brca pathway lead to abnormal centrosome amplification (30, 31), which is associated with genomic instability (32), we examined whether *HN-Smad4*$^{-/-}$ mucosa and HNSCC exhibited increased abnormal centrosome numbers. Since genomic instability is common at a certain stage in all tumors, we used papillomas induced by head and neck–specific *K-ras*^{G12D} mutation (8, 9) (hereafter referred to as *HN-K-ras*^{G12D} papillomas) for comparison with *HN-Smad4*$^{-/-}$ HNSCC. In wild-type mucosa, all cells exhibited 1 or 2 centrosomes (Figure 4A). *HN-K-ras*^{G12D} papillomas exhibited an increase in cells with 2 centrosomes, which corresponds with increased G_2/M phase cells, and 2.5% of cells with abnormal centrosome numbers (Figure 4A). By comparison, there were significantly more cells with abnormal centrosome numbers (31%) in *HN-Smad4*$^{-/-}$ HNSCCs. Additionally, *HN-Smad4*$^{-/-}$ mucosa exhibited a higher number of cells with abnormal centrosome numbers (5%) than *HN-Smad4*$^{+/+}$ mucosa or *HN-K-ras*^{G12D} papillomas (Figure 4A), suggesting that centrosome amplification is a cause rather than the consequence of tumorigenesis in *HN-Smad4*$^{-/-}$ head and neck epithelia.

We then performed array comparative genomic hybridization (aCGH) to assess genome-wide alterations in *HN-Smad4*$^{-/-}$ HNSCC. *HN-Smad4*$^{-/-}$ HNSCCs exhibited several consistent genomic aberrations, including regions commonly lost in human HNSCC. We observed loss of genetic material at 4qA5 (Figure 4B), which is syntenic to human 9p13 (33) and is associated with HNSCC metastases in humans (34). Additional regions included chromosomes 2qH4 and 3qF2 (Supplemental Table 1), which are syntenic to human 19p13 and 17q21, respectively, and are often lost in human HNSCC (35).

To further assess whether the above changes represented functional defects in the Fanc/Brca pathway as a result of *Smad4* deletion, we examined *Smad4*$^{-/-}$ keratinocytes for sensitivity to mitomycin C (MMC) killing. Fanc/Brca-deficient cells are hypersensitive to MMC due to failed replication resulting from unrepaired MMC-induced DNA crosslinks (36). While more than 90% of *Smad4*$^{+/+}$ cells were able to tolerate up to 40 ng/ml of MMC, only 50% of *Smad4*$^{-/-}$ keratinocytes survived after treatment with 5 ng/ml MMC (Figure 4C). Further, *Smad4*$^{-/-}$ keratinocytes that were able to survive after MMC treatment had a significant increase in chromosome breaks in comparison with *Smad4*$^{+/+}$ keratinocytes (Figure 4D; $P < 0.001$). These data suggest that *Smad4*$^{-/-}$ keratinoyctes are deficient in Fanc/Brca-mediated repair of crosslinker-induced DNA damage.

Smad4 loss plays a causal role in downregulation of the Fanc/Brca pathway and impairment of the Fanc/Brca DNA damage response. To further assess whether Smad4 loss plays a causal role in downregulation of Brca1, FancA, FancD2, and Rad51, we stably transfected a wild-type Smad4 expression construct into a Smad4-deficient HNSCC cell line (Cal27) that harbors a nonsense mutation in the *Smad4* gene (37). In response to Smad4 restoration in Cal27 cells (Cal27-Smad4 cells, Supplemental Figure 5), expression of Brca1 and Rad51 transcripts was increased by approximately 2-fold compared with parental Cal27 cells (Figure 5A). The expression of FancA and FancD2 was not significantly increased by Smad4 expression in Cal27 cells, which could be due to the fact that their reduction is not a primary

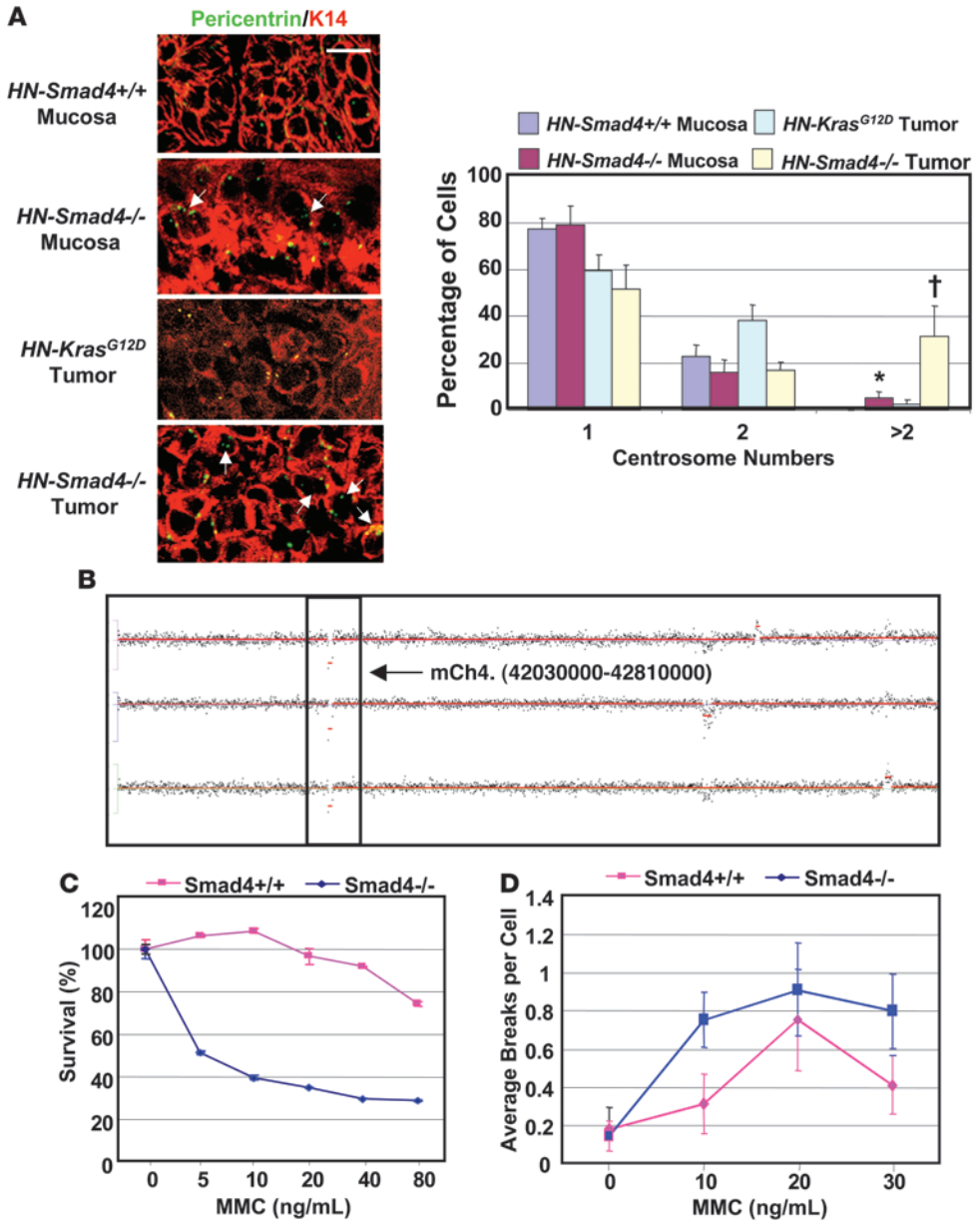

Figure 4

Abnormal centrosomes, increased genomic aberrations, and increased MMC sensitivity in *HN-Smad4*$^{-/-}$ mucosa and HNSCC. (**A**) Immunofluorescence for pericentrin (green or yellow). *HN-Smad4*$^{-/-}$ mucosa and HNSCCs have increased abnormal centrosome numbers compared with *HN-Smad4*$^{+/+}$ mucosa and control *HN-Smad4*$^{+/+}$ tumors (*HN-K-ras*^{G12D} papillomas), respectively. K14 (red) was used to counterstain epithelial cells. 3–5 samples per group were analyzed, and a representative image is presented. Arrows highlight cells with at least 3 centrosomes. The histogram summarizes quantification of centrosome numbers. 100–200 cells per group were analyzed. Error bars indicate SEM. $^{\dagger}P < 0.05$ versus *HN-Smad4*$^{+/+}$ tumors; $^{*}P < 0.05$ versus *HN-Smad4*$^{+/+}$ mucosa. Scale bar: 10 μm (all panels). (**B**) Chromosome 4 aCGH of 3 *HN-Smad4*$^{-/-}$ HNSCCs indicates that *HN-Smad4*$^{-/-}$ HNSCCs have several consistent genomic aberrations. The boxed region represents 2 copies of loss at chromosome 4qA5. (**C**) MMC sensitivity assay. Percent cell viability at increasing MMC concentrations indicates that *Smad4*$^{-/-}$ cells were significantly more sensitive to MMC than *Smad4*$^{+/+}$ cells. The experiment was run in triplicate, and error bars indicate SEM. $P < 0.05$ for all data points, other than 0 ng/ml, versus *Smad4*$^{+/+}$ cells. (**D**) Chromosome breakage assay. Plot of average chromosome breaks per cell for *Smad4*$^{+/+}$ and *Smad4*$^{-/-}$ cells at increasing MMC concentrations indicates that *Smad4*$^{-/-}$ cells have increased chromosome breaks compared with *Smad4*$^{+/+}$ cells. The experiments were run in triplicate, and error bars indicate SEM. $P < 0.001$ for all data points, other than 0 ng/ml, versus *Smad4*$^{+/+}$ cells.

effect of Smad4 loss or that other mechanisms regulate these molecules in HNSCC cancer cells. However, the latter is likely the case, as shown by an additional experiment in which we used siRNA to knock down Smad4 in normal primary human epidermal keratinocytes (HEKn). In response to approximately 75% Smad4 knockdown 48 hours after Smad4 siRNA treatment (Supplemental Figure 5), expression levels of Brca1, FancA, FancD2, and Rad51 were all reduced by approximately 50% in HEKn cells (Figure 5B).

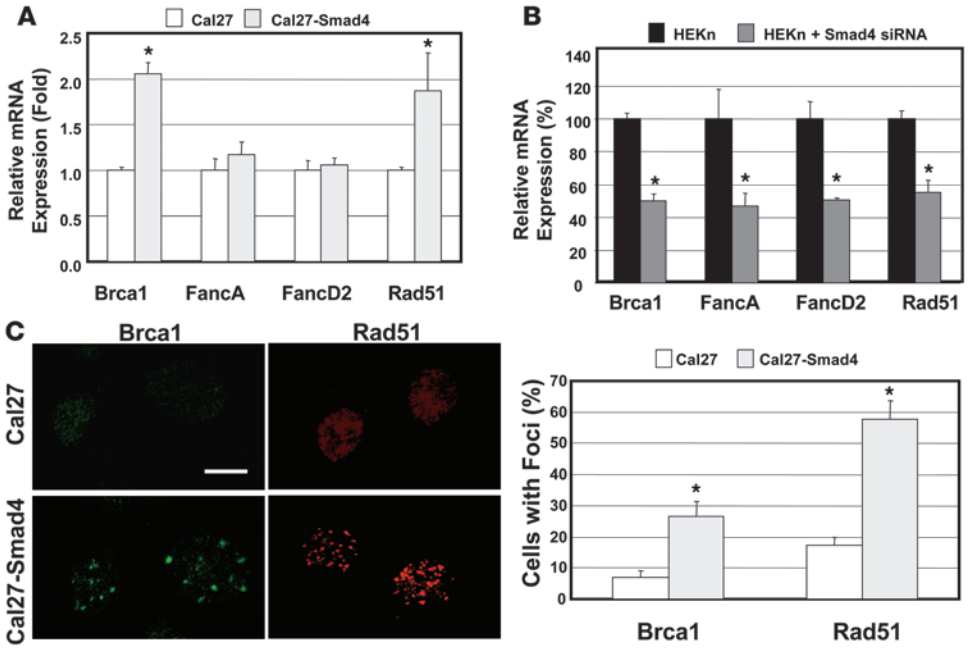

Figure 5

Fanc/Brca pathway gene expression and function correlate with Smad4 expression levels. (**A**) Relative expression levels of Fanc/Brca transcripts examined by qRT-PCR after Smad4 restoration in Smad4-deficient HNSCC cells (Cal27). Brca1 and Rad51 expression was increased by Smad4 restoration in Cal27 cells. The expression level of each gene in parental Cal27 was arbitrarily set at 100% for each experiment. Samples were run in triplicate for each experiment, and the mean relative expression levels from 3–4 independent experiments are presented. Error bars indicate SEM. *$P < 0.05$ versus parental Cal27 cells. (**B**) Relative expression levels of Fanc/Brca transcripts examined by qRT-PCR after Smad4 knockdown in normal keratinocytes (HEKn). Brca1, FancA, FancD2, and Rad51 expression was decreased after 48 hours of Smad4 siRNA treatment. The expression level of each gene in untreated HEKn cells was arbitrarily set at 100% for every experiment. Samples were run in triplicate for each experiment, and the mean relative expression levels from 3–4 independent experiments are presented. Error bars indicate SEM. *$P < 0.05$ versus untreated HEKn cells. (**C**) Brca1 and Rad51 nuclear foci detected by immunofluorescence in Cal27 and Cal27-Smad4 cells after MMC treatment. A representative image is presented. The histogram indicates the percentage of cells with Brca1 or Rad51 foci in Cal27 and Cal27-Smad4 cells. One hundred to 200 cells per group were analyzed. Error bars indicate SEM. *$P < 0.05$ versus Cal27. Scale bar: 5 μm (all panels).

To address whether rescued expression of Brca1 and Rad51 in Cal27 cells had functional consequences, we examined Brca1 and Rad51 DNA repair nuclear foci formation by immunofluorescence staining using the Cal27 and Cal27-Smad4 cells. Under normal conditions, Brca1 and Rad51 localize to sites of MMC-induced DNA damage with other members of the Fanc/Brca pathway to form DNA repair nuclear foci (38). After MMC treatment, only 10%–20% of Cal27 cells were able to form Brca1 and Rad51 foci, whereas Cal27-Smad4 cells exhibited a 3- to 4-fold increase in the number of cells able to form Brca1 and Rad51 foci (Figure 5C). These data suggest that Smad4 level affects not only expression levels of Fanc/Brca molecules, but also their function.

To determine whether Smad4 protein loss led to downregulation of Brca1 and Rad51 in human head and neck tissues, we assessed whether there was a correlation between Smad4 loss and Brca1 or Rad51 loss using IHC. As Akt is often overexpressed in human HNSCC (22, 39), we included Akt staining in the study. In general, the Akt staining pattern was similar in Smad4-positive and -negative lesions, i.e., mixed cytoplasmic and nuclear staining of cells in tumor epithelia and stroma (Figure 6). Interestingly, all Smad4-positive HNSCC and adjacent mucosa cases retained staining for Brca1 and Rad51 (Figure 6 and Table 1). Additionally, while Smad4-negative HNSCC and adjacent mucosa cases stained Akt to a similar extent as (if not more than) Smad4-positive cases, 80%–90% lost staining of Brca1 and Rad51 (Figure 6 and Table 1). These results represent a significant correlation between Smad4 loss and Brca1/Rad51 loss in both HNSCC and adjacent mucosa.

Smad4 loss led to increased inflammation. In addition to the above changes in *HN-Smad4*$^{-/-}$ epithelia, we observed numerous infiltrated leukocytes in the stroma of *HN-Smad4*$^{-/-}$ mucosa and HNSCC on histological sections and further examined the subtypes of infiltrated leukocytes using IHC. While inflammatory cells were rarely detected in the stroma of *HN-Smad4*$^{+/+}$ buccal tissues, both the stroma adjacent to *HN-Smad4*$^{-/-}$ buccal mucosa and the tumor stroma of *HN-Smad4*$^{-/-}$ HNSCC exhibited leukocyte infiltration comprising, in part, macrophages, granulocytes, and T lymphocytes (Figure 7A). Interestingly, Th17 cells, which represent a subset of proinflammatory T lymphocytes that are activated by TGF-β1 in mice (40, 41), were also detected in *HN-Smad4*$^{-/-}$ mucosa and HNSCC (Figure 7A).

We then assessed which inflammatory cytokines were activated in *HN-Smad4*$^{-/-}$ buccal mucosa and HNSCC, using a "Mouse Chemokines & Receptors" Superarray. Inflammatory cytokines were undetectable or present at very low levels in *HN-Smad4*$^{+/+}$ mucosa, but several cytokines were readily detected in *HN-Smad4*$^{-/-}$ mucosa and HNSCC (Figure 7B). Among them, MCP-1, MCP-2, and MIP-2 have been shown to be elevated by TGF-β1 overexpression in keratinocytes (42). These data are consistent with our previous observation that TGF-β1 overexpression alone in head and

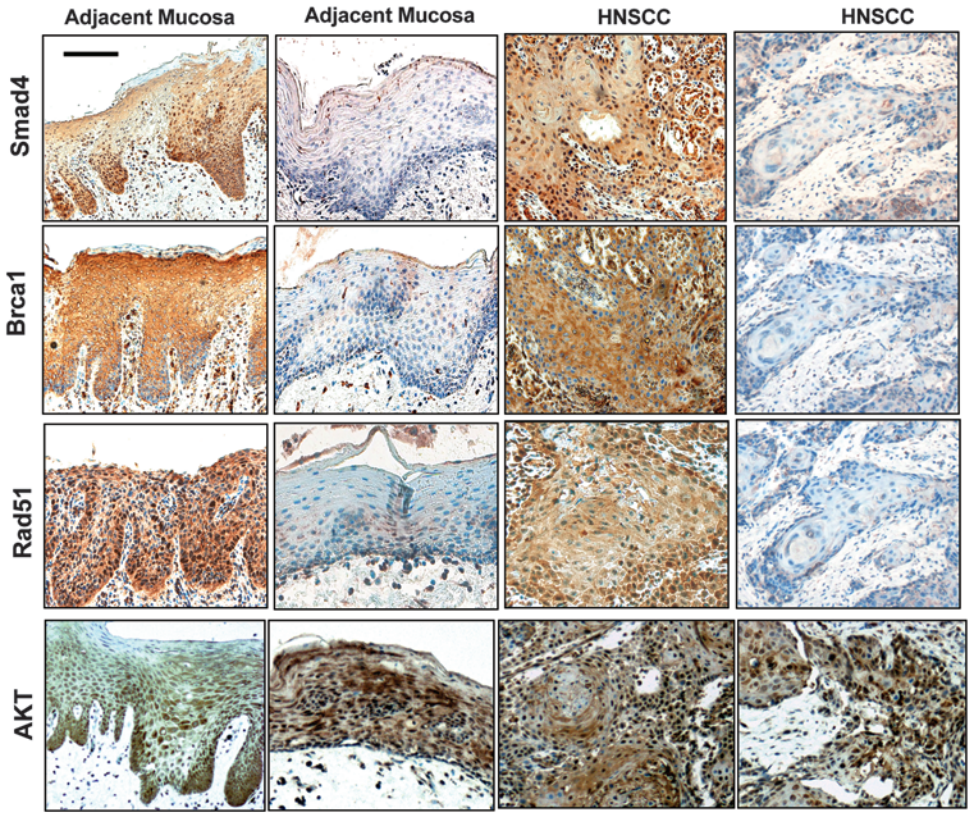

Figure 6
Human Fanc/Brca pathway protein expression correlates with Smad4 levels. IHC staining of Smad4, Brca1, Rad51, and Akt (brown) in HNSCC and adjacent mucosa samples. Mucosa adjacent to HNSCC and HNSCC samples from serial sections demonstrated a correlation between Smad4 loss and Brca1/Rad51 loss. Scale bar: 40 μm (all panels).

neck epithelial cells is sufficient to induce inflammation (43). To further assess whether *HN-Smad4*$^{-/-}$ tissues had compensatory TGF-β1 overexpression as a result of Smad4 loss, we performed an ELISA for total TGF-β1. *HN-Smad4*$^{-/-}$ HNSCCs expressed significantly more TGF-β1 (514 pg/mg total protein) than *HN-Smad4*$^{+/+}$ buccal mucosa (84 pg/mg total protein) (Figure 8A). Interestingly, *HN-Smad4*$^{-/-}$ buccal mucosa also exhibited significantly more TGF-β1 (156 pg/mg total protein) than *HN-Smad4*$^{+/+}$ mucosa (Figure 8A), indicating that the Smad4 loss–associated increase in TGF-β1 occurred early on in tumorigenesis. To determine whether increased TGF-β1 conferred downstream signaling activation, we performed immunostaining of signaling Smads in *HN-Smad4*$^{-/-}$ mucosa and HNSCC. Interestingly, while loss of nuclear phospho-Smad2 (pSmad2) was evident in *HN-Smad4*$^{-/-}$ mucosa and HNSCC, increased nuclear staining for Smad3 and pSmad1/5/8 was observed in *HN-Smad4*$^{-/-}$ buccal mucosa and HNSCC compared with *HN-Smad4*$^{+/+}$ mucosa (Figure 8B).

Based on our previous study suggesting that Smad3 is a key mediator in TGF-β1–associated inflammation (44), we assessed whether increased TGF-β1 and Smad3 nuclear staining represented functional activation that contributed to inflammation in *HN-Smad4*$^{-/-}$ tissues. We crossed *HN-Smad4*$^{-/-}$ mice into a *Smad3*$^{+/-}$ background (44) to generate compound *HN-Smad4*$^{-/-}$*Smad3*$^{+/-}$ mice. Smad4 deletion was induced at 3 weeks, and mice were euthanized at 4 weeks of age for excision of head and neck tissues. *HN-Smad4*$^{-/-}$ tissues exhibited inflammation 1 week after Smad4 was deleted, with infiltrated leukocytes consisting mainly of macrophages and granulocytes, as well as sporadic T lymphocytes (CD3^{+}) (Figure 8C). Interestingly, leukocyte infiltration in *HN-Smad4*$^{-/-}$ tissues was markedly reduced in *HN-Smad4*$^{-/-}$*Smad3*$^{+/-}$ tissues (Figure 8C), suggesting that Smad3-dependent TGF-β1 signaling contributed at least in part to inflammation in *HN-Smad4*$^{-/-}$ tissues.

Discussion

Early-stage Smad4 loss plays a causal role in HNSCC tumorigenesis. In the current study, we found that *SMAD4* mRNA levels were significantly reduced in human HNSCCs and in grossly normal buccal mucosa adjacent to HNSCC. Among them, we detected 33% LOH at the Smad4 locus, which is similar to previous reports (3, 4). In these cases, genetic loss of the first allele may contribute to at least 50% of Smad4 downregulation, as mice with heterozygous deletion of Smad4 exhibited approximately 50% loss of transcript and protein (22–24). Smad4 levels can be further downregulated if the remaining allele is mutated. Additionally, epigenetic, posttranscriptional, and posttranslational modifications could contribute to further loss of the remaining Smad4 expression. In contrast to other cancer types in which Smad4 is downregulated or lost at malignant stages, frequent Smad4 downregulation in grossly normal buccal mucosa adjacent to HNSCC suggests an early role of Smad4 reduction in HNSCC tumorigenesis. This notion is further supported by spontaneous HNSCC formation in mice with *Smad4* deletion specifically in head and neck epithelia. This is somewhat surprising, since patients

Table 1
Correlation between Smad4 and Brca1/Rad51 expression in adjacent mucosa and HNSCC

Sample	Smad4+	Smad4−
Brca1 loss		
Mucosa adjacent to HNSCC	0/8 (0%)	12/13 (92%)[A]
HNSCC	0/8 (0%)	21/24 (88%)[A]
Rad51 loss		
Mucosa adjacent to HNSCC	0/8 (0%)	12/13 (92%)[A]
HNSCC	0/8 (0%)	20/24 (83%)[A]

[A]$P < 0.05$ versus Smad4+.

with juvenile polyposis coli, a syndrome characterized by multiple benign colon polyps as a result of germline heterozygous Smad4 loss, do not exhibit an increased risk for HNSCC. This could reflect the tissue specificity of the germline mutation and indicates that additional molecular alterations in keratinocytes must be required for HNSCC formation in *HN-Smad4*$^{-/-}$ mice. Interestingly, grossly normal *HN-Smad4*$^{-/-}$ mucosa exhibited increased abnormal centrosome numbers and reduced expression of Fanc/Brca genes, suggesting that homozygous Smad4 loss, through initiation of genomic instability, may generate secondary oncogenic changes necessary for tumorigenesis. For example, we found that a subset of *HN-Smad4*$^{-/-}$ HNSCCs exhibited *Ras* mutations, which have been associated with HNSCC initiation (8, 9). Since mice with head and neck–specific TGFβR2 deletion do not develop spontaneous HNSCC unless a mutant *Ras* is introduced (8), spontaneous *Ras* mutation appears to be infrequent in mouse head and neck epithelia but could be a consequence of Smad4 loss–mediated genomic instability. While neither heterozygous deletion of *Smad4* in the current study nor *K-ras* mutation alone (8) are able to lead to HNSCC formation, *K-ras*^{G12D}*Smad4*$^{+/-}$ mice rapidly developed HNSCC, indicating that early genetic *Ras* activation is able to initiate HNSCC formation with heterozygous *Smad4* loss. These data also suggest that single-copy loss of *Smad4* in the setting of other oncogenic changes, i.e., the "field cancerization" observed in HNSCC patients (1), is sufficient for HNSCC tumorigenesis. Thus, approximately 50% loss of *Smad4* mRNA at either the genomic or transcriptional level could be sufficient for tumorigenesis in these cases. Further, although we have not detected EGFR amplification in *HN-Smad4*$^{-/-}$ HNSCCs as seen in human patients (1), Ras activation could exert similar effects. It remains to be determined whether other genetic alterations found in *HN-Smad4*$^{-/-}$ HNSCCs also cause tumor initiation.

Smad4 loss contributes to defects in the Fanc/Brca pathway and genomic instability. It has been shown that Fanconi anemia patients, who carry germline mutations in Fanc/Brca pathway genes, have a high incidence of HNSCC at a young age (10). Moreover, Fanc/Brca pathway–associated genes are downregulated in sporadic HNSCC (6, 35, 45, 46). Additionally, mice with epithelia-specific heterozygous knockout of *Brca1* developed oral SCCs, indicating that Brca1 loss plays an important role in HNSCC tumorigenesis (47). In the current study, downregulation of Fanc/Brca pathway genes was detected in both grossly normal buccal mucosa and HNSCC lesions of *HN-Smad4*$^{-/-}$ mice. Smad4 knockdown led to reduction in Fanc/Brca gene expression, and restoration of normal Smad4 in a Smad4-deficient HNSCC cell line increased expression of Fanc/Brca pathway genes. Additionally, the majority of Smad4-deficient mucosa and HNSCC clinical samples demonstrated loss of both Brca1 and Rad51. Thus, our data suggest a causal role for Smad4 loss in downregulation of the Fanc/Brca pathway. It remains to be determined whether Smad4 regulates any of the Fanc/Brca family members via direct transcriptional activation, or via other regulators downstream of Smad4. Nevertheless, Smad4 loss appeared to be sufficient to cause functional defects in the Fanc/Brca pathway. This is evidenced by increased sensitivity to MMC killing and chromosome breakage in *Smad4*$^{-/-}$ primary cells and defects in Rad51/Brca1 nuclear foci formation in Smad4-deficient HNSCC cells. Defects in the Fanconi pathway lead to increased genomic instability in Fanconi anemia patients (38) and could be responsible for the increased abnormal centrosome numbers and genomic aberrations observed in *HN-Smad4*$^{-/-}$ HNSCC. Consistent with our observations, both Brca1-deficient cells (31) and cells expressing a dominant-negative form of Rad51 (30) exhibited increased centrosome numbers and chromosomal aberrations. In contrast to our current study, TGF-β1–treated Mv1Lu cells show decreased Rad51 protein and Rad51 nuclear foci in a Smad4-dependent manner (48). It is possible that Smad4 functions differently in different cell types. Additionally, increased TGF-β1/Smad3 in *HN-Smad4*$^{-/-}$ tissues could contribute to downregulation of the Fanc/Brca pathway. In support of the latter hypothesis, Smad3 has been shown to bind to the Brca1 protein and inhibit Brca1 nuclear foci formation and DNA repair efficiency (49). Thus, genomic instability coupled with hyperproliferation and reduced apoptosis may allow *HN-Smad4*$^{-/-}$ cells to escape from DNA damage–induced cell death during tumorigenesis.

Smad4 loss results in increased inflammation. Human HNSCCs often exhibit chronic inflammation (1, 50). It has been reported that Smad4 deletion in T cells, but not in gastrointestinal epithelia, resulted in gastrointestinal cancer associated with increased inflammation and other tumor-promoting stromal changes (51). This study is consistent with the notion that TGF-β signaling in T cells has an antiinflammatory and immunosuppressive effect. However, it has also been shown that Smad4 loss in intestinal epithelia led to increased inflammation that promoted tumor invasion (15). Consistent with the latter study, our findings show that loss of *Smad4* in both tumor epithelia and grossly normal-appearing mucosa adjacent to the tumor led to marked inflammation that was associated with increased TGF-β1. Additionally, loss of Smad4 in head and neck epithelia as early as 1 week after *Smad4* was deleted led to inflammation, which was not observed in *Kras* mutant papillomas (8), suggesting that inflammation was initiated by epithelial Smad4 loss. We have shown that TGF-β1 is overexpressed in human HNSCC and that overexpression of *TGFB1* in head and neck epithelia resulted in marked inflammation (43). Our previous study has shown that TGF-β1 overexpression in HNSCC with TGFβR2 deletion induces inflammation via its effects on tumor stroma, as TGF-β1 cannot activate downstream Smads in tumor epithelia as a result of TGFβR2 loss (8). Interestingly, in contrast to that model, we also detected increased nuclear Smad1/5/8 and Smad3 in epithelial cells of *HN-Smad4*$^{-/-}$ buccal mucosa and HNSCC. Activation of Smad1 and Smad5 correlated with inflammation in allergic airway epithelia (52), and abrogation of TGF-β1 signaling has been shown to activate Smad1 and Smad5, which correlated with increased tumor invasion (53). A recent report shows that TGF-β1 overexpression is able to stimulate Smad1 and Smad5 phosphorylation in tumorigenic cells, which promotes cell migration (54). Thus, increased nuclear Smad1/5/8 may play a role in the inflammatory and invasive phenotype observed in *HN-Smad4*$^{-/-}$ HNSCC. Unlike

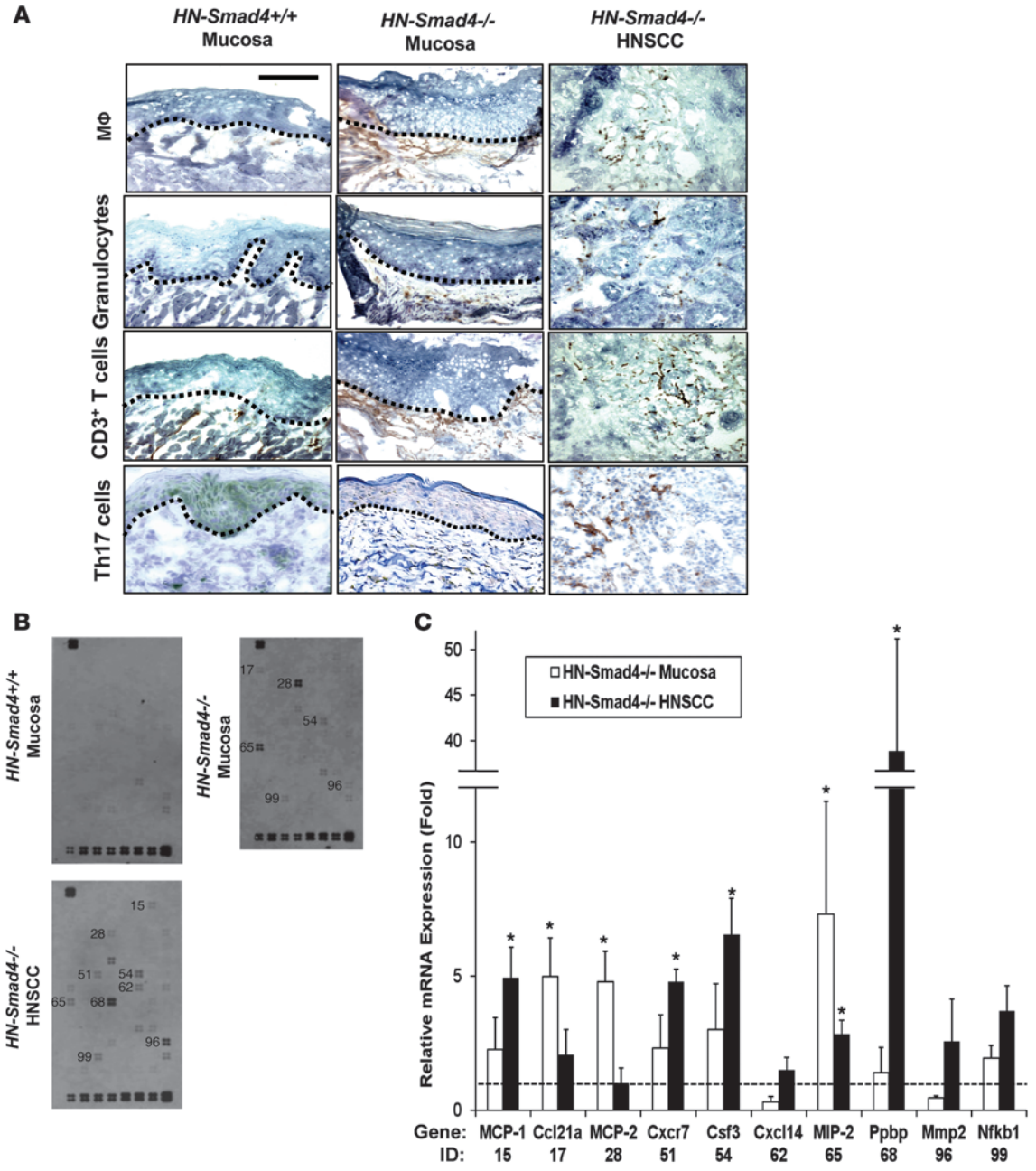

Figure 7

Increased inflammation and inflammatory chemokines in *HN-Smad4*$^{-/-}$ lesions. (**A**) Immunostaining of *HN-Smad4*$^{+/+}$ mucosa, *HN-Smad4*$^{-/-}$ mucosa, and *HN-Smad4*$^{-/-}$ HNSCCs with leukocyte markers. Macrophages (Mϕ) were stained with antibodies against F4/80; granulocytes with antibodies against Ly6G; T cells with antibodies against CD11b; and Th17 cells with antibodies against IL-17. The black dotted lines indicate the boundary between mucosa and stroma. *HN-Smad4*$^{-/-}$ mucosa has increased inflammatory markers in the underlying stroma compared with *HN-Smad4*$^{+/+}$ mucosa, and *HN-Smad4*$^{-/-}$ HNSCCs have marked inflammation in the tumor stroma. 5–7 samples from each group were analyzed, and a representative image is presented. Scale bar: 40 μm (all panels). (**B**) Pathway-specific "Mouse Chemokines & Receptors" Superarray revealed increased inflammatory molecules in *HN-Smad4*$^{-/-}$ mucosa and HNSCC compared with *HN-Smad4*$^{+/+}$ mucosa. Three samples per group of *HN-Smad4*$^{+/+}$ mucosa, *HN-Smad4*$^{-/-}$ mucosa, and *HN-Smad4*$^{-/-}$ HNSCC were examined, and a representative blot from each group is presented. Genes with visible differences compared with *HN-Smad4*$^{+/+}$ mucosa are labeled to the left with numbers that correspond to gene IDs quantified in **C**. (**C**) Relative mRNA expression (fold change) for each gene was calculated as optical density above adjacent background for *HN-Smad4*$^{-/-}$ mucosa and *HN-Smad4*$^{-/-}$ HNSCC samples compared with *HN-Smad4*$^{+/+}$ samples. Gene names and IDs corresponding to numbers on the blot in **B** are displayed below. Error bars indicate SEM. *$P < 0.05$ versus *HN-Smad4*$^{+/+}$ mucosa samples.

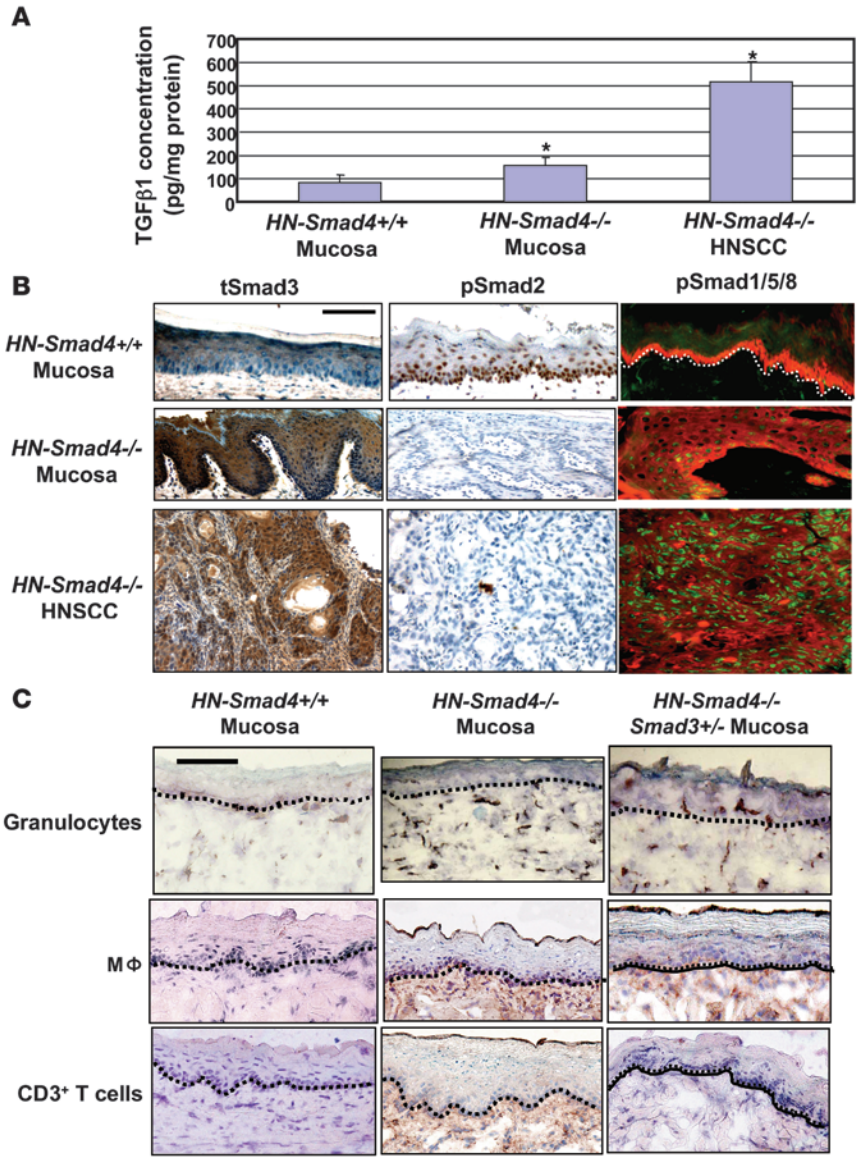

Figure 8
Increased TGF-β1 and activation of Smad1/5/8 and Smad3 in *HN-Smad4*$^{-/-}$ lesions. (**A**) ELISA for total TGF-β1 protein. Each group contains 5–7 samples. Error bars indicate SEM. *$P < 0.05$ versus *HN-Smad4*$^{+/+}$ mucosa. (**B**) Immunostaining of *HN-Smad4*$^{+/+}$ buccal mucosa, *HN-Smad4*$^{-/-}$ buccal mucosa, and *HN-Smad4*$^{-/-}$ HNSCC for pSmad2, total Smad3 (tSmad3), and pSmad1/5/8. pSmad2 was decreased, while nuclear Smad3 and pSmad1/5/8 were increased in both *HN-Smad4*$^{-/-}$ mucosa and *HN-Smad4*$^{-/-}$ HNSCC. The white dotted line in the upper-right panel represents the boundary between mucosa and stroma. Five to 7 samples from each group were examined, and a representative image is presented. (**C**) Immunostaining of *HN-Smad4*$^{+/+}$ mucosa, *HN-Smad4*$^{-/-}$ mucosa, and *HN-Smad4*$^{-/-}$*Smad3*$^{+/-}$ mucosa with leukocyte markers (brown) of macrophages (CD11b), granulocytes (Ly6G), and CD3^{+} T cells. The black dotted lines indicate the boundary between mucosa and stroma. *HN-Smad4*$^{+/+}$ mucosa exhibited a few granulocytes but no macrophages or T cells. All 3 types of leukocytes are evident in *HN-Smad4*$^{-/-}$ mucosa but are attenuated in *HN-Smad4*$^{-/-}$*Smad3*$^{+/-}$ mucosa. Scale bar: 40 μm (all panels).

Smad2 and Smad4, Smad3 has a tumor-promoting role under certain circumstances (55). We have shown that Smad3 is important in mediating TGF-β–induced inflammation and expression of activating protein 1 (AP-1) family members (44). In the current study, inflammation in *HN-Smad4*$^{-/-}$ tissues was markedly attenuated in a Smad3-heterozygous background, suggesting that Smad3 mediates, at least in part, increased TGF-β1–associated inflammation. In addition to inducing changes in cytokines critical for HNSCC tumorigenesis (56, 57), inflammation and the resultant production of reactive oxygen species have been linked to the generation of genomic instability (58). Thus, Smad4 loss–associated inflammation may also contribute to the genomic instability observed in our model.

In summary, we found that Smad4 was downregulated at the pretranslational level early in human HNSCC tumorigenesis, which correlated with downregulation of Brca1 and Rad51. We present a model wherein Smad4 loss results in spontaneous HNSCC formation. Our results indicate that Smad4 loss contributes to increased genomic instability in tumor epithelia. This effect, coupled with abrogation of TGF-β–induced growth inhibition and apoptosis but enhancement of TGF-β–mediated inflammation, could allow expansion of genetically damaged cells during HNSCC tumorigenesis. Our study also suggests potential therapeutic strategies for HNSCC with Smad4 loss. For instance, since Fanc/Brca-defective cells exhibit increased sensitivity to radiation (59) and poly(ADP-ribose) polymerase inhibitor–induced cell death (38, 60), our study will encourage future investigation into whether these approaches, coupled with control of excessive inflammation, will be effective treatments for patients with Smad4-deficient HNSCC. We believe the mouse model presented here will be an ideal tool for testing novel therapeutic interventions.

Methods

For experimental procedures not described herein, see Supplemental Methods.

Patients. HNSCC and case-matched adjacent tissue samples were surgically resected between the years 2000 and 2005 from consenting patients at the OHSU Department of Otolaryngology under an Institutional Review

Board–approved protocol. Tissues examined in this study included 21 oral cavity SCCs, 9 larynx SCCs, 5 oropharynx SCCs, 1 nasal cavity SCC, and case-matched tissues adjacent to tumors. Seven normal oropharynx samples from sleep apnea patients were used as normal controls.

Cell culture and transfections. Primary *Smad4*$^{-/-}$ and *Smad4*$^{+/+}$ cell lines were generated from neonatal compound *K5.CrePR1/Smad4*$^{f/f}$ or monogenic *Smad4*$^{f/f}$ or *Smad4*$^{f/w}$ control mice after being exposed in utero to RU486 to accomplish Smad4 deletion in bigenic mice. Cell lines were generated by CellNTec (Millipore) and were cultured in keratinocyte-specific medium Cnt07 (Chemicon). Human tongue SCC line Cal27 was purchased from ATCC and cultured in DMEM (ATCC) with 10% FBS. To create Cal27 lines stably expressing Smad4 (Cal27-Smad4), Cal27 cells were transfected with pcDNA Flag-Smad4M purchased from Addgene, using Lipofectamine 2000 Transfection Reagent (Invitrogen), and selected in G418 (Sigma-Aldrich) for 4 weeks. To knock down Smad4 in HEKn cells (HEKn plus *Smad4* siRNA), HEKn cells were treated with Stealth RNAi against Smad4 (5′-GGUGAUGUUUGGGUCAGGUGCCUUA-3′) from Invitrogen using XtremeGENE siRNA Transfection Reagent (Roche) for 48 hours, then harvested.

Histology and immunostaining. Samples were fixed in 10% neutral buffered formalin, embedded, sectioned, and stained with H&E as we have previously described (8). Tumor types were determined based on the criteria described previously (8). Immunohistochemical staining was performed on frozen or paraffin-embedded sections using antibodies against Brca1, Rad51, CD3, Smad4, and Smad3 (Santa Cruz Biotechnology Inc.); pSmad2 and total Akt1 (Cell Signaling Technology); Ly-6G (eBioscience); F4/80 (Caltag Laboratories); CD11b, IL-17 (BD Biosciences — Pharmingen); and Ras (Abcam) as we have previously described (8). Sections were counterstained with hematoxylin. Evaluation of Smad4, Brca1, and Rad51 staining of human HNSCC samples was performed by 2 independent investigators using the methods described previously (8). Double immunofluorescence staining was performed as we have described previously (8). Primary antibodies included K13 (RDI), Keratin 14 (Fitzgerald), Pericentrin (Covance), pSmad1/5/8 (Cell Signaling Technology), and PCNA (Santa Cruz Biotechnology Inc.). The sections were incubated with Alexa Fluor 488–conjugated (green) or Alexa Fluor 594–conjugated (red) secondary antibodies (Invitrogen). Centrosome immunofluorescence images were captured using confocal microscopy with a Leica SP2 confocal microscope (Leica Microsystems Inc.).

qRT-PCR. Total RNA was isolated using TRIzol (Invitrogen) and further purified using a QIAGEN RNeasy Mini kit as previously described (8). One hundred nanograms of RNA from each sample was subjected to qRT-PCR using Brilliant II QRT-PCR 1-Step Master Mix (Stratagene) and TaqMan Assays-on-Demand probes (Applied Biosystems). An 18S, Keratin 14, or Gapdh probe was used as an internal control. Each sample was examined in triplicate. The relative RNA expression levels were determined by normalizing with internal controls, the values of which were calculated using the comparative Ct method.

Nuclear foci immunofluorescence. Cells were cultured on chamber slides and treated with 20 ng/ml MMC (Sigma-Aldrich) for 24 hours. Cells were then fixed with 4% paraformaldehyde, permeabilized with 0.3% Triton X-100, digested in pepsin solution (Lab Vision, Thermo Scientific), blocked for 1 hour with 10% normal goat serum plus 0.1% NP-40, and incubated with Brca1 (Santa Cruz Biotechnology Inc.) or Rad51 (Santa Cruz Biotechnology Inc.) primary antibodies overnight. Alexa Fluor 488– or 594–conjugated secondary antibodies (Invitrogen) were used for immunofluorescence staining, and images were taken using confocal microscopy with a Leica SP2 confocal microscope (Leica Microsystems Inc.).

aCGH. Mouse Whole-genome comparative genomic hybridization (CGH) arrays (NimbleGen Systems Inc.) comprising 50–75mer oligo probes based on UCSC build MM8, with a median probe spacing of 5,782 bp, were utilized to examine tumors for chromosomal aberrations. Genomic DNA from 5 *HN-Smad4*$^{-/-}$ HNSCCs was isolated, fluorescently labeled, and hybridized to arrays. Tumor gene copy numbers were determined by comparison with reference DNA isolated from normal C57BL/6 mice after competitive hybridization. Data were analyzed with SignalMap software (Nimblegen Systems Inc.) to identify deleted and amplified regions.

MMC sensitivity assay. Cells were seeded at a density of 10,000 cells/ml into 24-well plates and treated the next day in triplicate with the indicated concentrations of MMC for 4 days. An MTT assay (Chemicon) was performed to assess for cell viability using the manufacturer's instructions.

Chromosome breakage analysis. Chromosome breakage analysis was performed by the OHSU Cytogenetics Core. Cell cultures were treated with indicated concentrations of MMC (Sigma-Aldrich) in triplicate for 48 hours in the dark. Cells were then harvested after a 3-hour exposure to colcemid (0.05 μg/ml; Invitrogen). Following a 10-minute treatment with hypotonic solution (0.075 M KCl, 5% fetal calf serum), the cells were fixed with a 3:1 mixture of methanol:acetic acid. Cells were dropped onto microscope slides for metaphase spreads and stained with Wright's stain (Fisher Scientific) for 3 minutes. Fifty metaphase figures from each culture were scored for chromosome breaks. Radial formations were not included in the calculations.

Superarray. RNA was amplified and labeled using Affymetrix protocols (http://www.affymetrix.com/support/technical/manual/expression_manual.affx) with the help of the OHSU Affymetrix Microarray Core and hybridized against the Oligo GEArray Mouse Chemokines & Receptors (Superarray). Membranes were washed and incubated with a Streptavidin Alexa Fluor 680–conjugated antibody (Invitrogen) and scanned with the Odyssey Infrared Imaging System (LI-COR Biosciences).

TGF-β1 ELISA. A TGF-β1–specific ELISA kit (R&D Systems) was used to quantify levels of TGF-β1 ligand. Protein samples were extracted as previously described (42), acidified with 1N HCl, and neutralized with 1.2N NaOH/0.5 M HEPES to assay for the total amount of TGF-β1 protein (both latent and active forms).

Statistics. Statistical differences between 2 groups of data were analyzed using 2-tailed Student's *t* test with the exceptions of centrosome quantification in Figure 4A, foci quantification in Figure 5C, and the data in Table 1, which were calculated using a 2-tailed Fisher's exact test; and the chromosome breakage data in Figure 4D, which was calculated using a χ^2 test. The data are presented as mean ± SEM. *P* values less than 0.05 were considered significant.

Acknowledgments

The authors thank Yuexin Li and Donna Wang for their technical assistance. This work was supported by NIH grants to X.-J. Wang and by an Oregon Medical Research Foundation grant to S.-L. Lu. S.-L. Lu is an investigator of the THANC (Thyroid, Head and Neck Cancer) Foundation. S. Bornstein and S. Malkoski are recipients of NIH training grants.

Received for publication February 9, 2009, and accepted in revised form August 5, 2009.

Address correspondence to: Shi-Long Lu, Department of Otolaryngology, Bldg. RC-2, Rm P15-7112, Mail Stop 8116, University of Colorado Denver, Aurora, Colorado 80045-0508, USA. Phone: (303) 724-0784; Fax: (303) 724-4553; E-mail: shi-long.lu@ucdenver.edu. Or to: Xiao-Jing Wang, Department of Pathology, Bldg. RC1-N, Rm P18-5128, Mail Stop 8104, University of Colorado Denver, Aurora, Colorado 80045-0508, USA. Phone: (303) 724-3001; Fax: (303) 724-4730; E-mail: xj.wang@ucdenver.edu.

1. Hunter, K.D., Parkinson, E.K., and Harrison, P.R. 2005. Profiling early head and neck cancer. *Nat. Rev. Cancer.* **5**:127–135.
2. Forastiere, A., Koch, W., Trotti, A., and Sidransky, D. 2001. Head and neck cancer. *N. Engl. J. Med.* **345**:1890–1900.
3. Takebayashi, S., et al. 2000. Identification of new minimally lost regions on 18q in head and neck squamous cell carcinoma. *Cancer Res.* **60**:3397–3403.
4. Kim, S.K., et al. 1996. DPC4, a candidate tumor suppressor gene, is altered infrequently in head and neck squamous cell carcinoma. *Cancer Res.* **56**:2519–2521.
5. Papadimitrakopoulou, V.A., et al. 1998. Presence of multiple incontiguous deleted regions at the long arm of chromosome 18 in head and neck cancer. *Clin. Cancer Res.* **4**:539–544.
6. Sparano, A., et al. 2006. Genome-wide profiling of oral squamous cell carcinoma by array-based comparative genomic hybridization. *Laryngoscope.* **116**:735–741.
7. Lu, S.L., Herrington, H., and Wang, X.J. 2006. Mouse models for human head and neck squamous cell carcinomas. *Head Neck.* **28**:945–954.
8. Lu, S.L., et al. 2006. Loss of transforming growth factor-beta type II receptor promotes metastatic head-and-neck squamous cell carcinoma. *Genes Dev.* **20**:1331–1342.
9. Caulin, C., et al. 2004. Inducible activation of oncogenic K-ras results in tumor formation in the oral cavity. *Cancer Res.* **64**:5054–5058.
10. Kutler, D.I., et al. 2003. High incidence of head and neck squamous cell carcinoma in patients with Fanconi anemia. *Arch. Otolaryngol. Head Neck Surg.* **129**:106–112.
11. Hahn, S.A., et al. 1996. DPC4, a candidate tumor suppressor gene at human chromosome 18q21.1. *Science.* **271**:350–353.
12. Zhang, Y., Feng, X., We, R., and Derynck, R. 1996. Receptor-associated Mad homologues synergize as effectors of the TGF-beta response. *Nature.* **383**:168–172.
13. Siegel, P.M., and Massague, J. 2003. Cytostatic and apoptotic actions of TGF-beta in homeostasis and cancer. *Nat. Rev. Cancer.* **3**:807–821.
14. Bierie, B., and Moses, H.L. 2006. TGF-beta and cancer. *Cytokine Growth Factor Rev.* **17**:29–40.
15. Kitamura, T., et al. 2007. SMAD4-deficient intestinal tumors recruit CCR1+ myeloid cells that promote invasion. *Nat. Genet.* **39**:467–475.
16. Takaku, K., et al. 1998. Intestinal tumorigenesis in compound mutant mice of both Dpc4 (Smad4) and Apc genes. *Cell.* **92**:645–656.
17. Izeradjene, K., et al. 2007. Kras(G12D) and Smad4/Dpc4 haploinsufficiency cooperate to induce mucinous cystic neoplasms and invasive adenocarcinoma of the pancreas. *Cancer Cell.* **11**:229–243.
18. Bardeesy, N., et al. 2006. Smad4 is dispensable for normal pancreas development yet critical in progression and tumor biology of pancreas cancer. *Genes Dev.* **20**:3130–3146.
19. Teng, Y., et al. 2006. Synergistic function of Smad4 and PTEN in suppressing forestomach squamous cell carcinoma in the mouse. *Cancer Res.* **66**:6972–6981.
20. Xu, X., et al. 2006. Induction of intrahepatic cholangiocellular carcinoma by liver-specific disruption of Smad4 and Pten in mice. *J. Clin. Invest.* **116**:1843–1852.
21. Xu, X., et al. 2000. Haploid loss of the tumor suppressor Smad4/Dpc4 initiates gastric polyposis and cancer in mice. *Oncogene.* **19**:1868–1874.
22. Qiao, W., et al. 2006. Hair follicle defects and squamous cell carcinoma formation in Smad4 conditional knockout mouse skin. *Oncogene.* **25**:207–217.
23. Li, W., et al. 2003. Squamous cell carcinoma and mammary abscess formation through squamous metaplasia in Smad4/Dpc4 conditional knockout mice. *Development.* **130**:6143–6153.
24. Yang, L., et al. 2005. Targeted disruption of Smad4 in mouse epidermis results in failure of hair follicle cycling and formation of skin tumors. *Cancer Res.* **65**:8671–8678.
25. Snijders, A.M., et al. 2005. Rare amplicons implicate frequent deregulation of cell fate specification pathways in oral squamous cell carcinoma. *Oncogene.* **24**:4232–4242.
26. Fukuchi, M., et al. 2002. Decreased Smad4 expression in the transforming growth factor-beta signaling pathway during progression of esophageal squamous cell carcinoma. *Cancer.* **95**:737–743.
27. Natsugoe, S., et al. 2002. Smad4 and transforming growth factor beta1 expression in patients with squamous cell carcinoma of the esophagus. *Clin. Cancer Res.* **8**:1838–1842.
28. Bloor, B.K., Su, L., Shirlaw, P.J., and Morgan, P.R. 1998. Gene expression of differentiation-specific keratins (4/13 and 1/10) in normal human buccal mucosa. *Lab. Invest.* **78**:787–795.
29. Rodriguez-Viciana, P., et al. 2005. Cancer targets in the Ras pathway. *Cold Spring Harb. Symp. Quant. Biol.* **70**:461–467.
30. Bertrand, P., Lambert, S., Joubert, C., and Lopez, B.S. 2003. Overexpression of mammalian Rad51 does not stimulate tumorigenesis while a dominant-negative Rad51 affects centrosome fragmentation, ploidy and stimulates tumorigenesis, in p53-defective CHO cells. *Oncogene.* **22**:7587–7592.
31. Xu, X., et al. 1999. Centrosome amplification and a defective G2-M cell cycle checkpoint induce genetic instability in BRCA1 exon 11 isoform-deficient cells. *Mol. Cell.* **3**:389–395.
32. Fukasawa, K. 2007. Oncogenes and tumour suppressors take on centrosomes. *Nat. Rev. Cancer.* **7**:911–924.
33. Wreesmann, V.B., et al. 2004. Identification of novel prognosticators of outcome in squamous cell carcinoma of the head and neck. *J. Clin. Oncol.* **22**:3965–3972.
34. Wreesmann, V.B., et al. 2004. Genetic abnormalities associated with nodal metastasis in head and neck cancer. *Head Neck.* **26**:10–15.
35. Weber, F., et al. 2007. Microenvironmental genomic alterations and clinicopathological behavior in head and neck squamous cell carcinoma. *JAMA.* **297**:187–195.
36. Kennedy, R.D., and D'Andrea, A.D. 2005. The Fanconi Anemia/BRCA pathway: new faces in the crowd. *Genes Dev.* **19**:2925–2940.
37. Qiu, W., Schonleben, F., Li, X., and Su, G.H. 2007. Disruption of transforming growth factor beta-Smad signaling pathway in head and neck squamous cell carcinoma as evidenced by mutations of SMAD2 and SMAD4. *Cancer Lett.* **245**:163–170.
38. D'Andrea, A.D., and Grompe, M. 2003. The Fanconi anaemia/BRCA pathway. *Nat. Rev. Cancer.* **3**:23–34.
39. Amornphimoltham, P., et al. 2004. Persistent activation of the Akt pathway in head and neck squamous cell carcinoma: a potential target for UCN-01. *Clin. Cancer Res.* **10**:4029–4037.
40. Mangan, P.R., et al. 2006. Transforming growth factor-beta induces development of the T(H)17 lineage. *Nature.* **441**:231–234.
41. Veldhoen, M., Hocking, R.J., Atkins, C.J., Locksley, R.M., and Stockinger, B. 2006. TGFbeta in the context of an inflammatory cytokine milieu supports de novo differentiation of IL-17-producing T cells. *Immunity.* **24**:179–189.
42. Li, A.G., Wang, D., Feng, X.H., and Wang, X.J. 2004. Latent TGFbeta1 overexpression in keratinocytes results in a severe psoriasis-like skin disorder. *EMBO J.* **23**:1770–1781.
43. Lu, S.L., et al. 2004. Overexpression of transforming growth factor beta1 in head and neck epithelia results in inflammation, angiogenesis, and epithelial hyperproliferation. *Cancer Res.* **64**:4405–4410.
44. Li, A.G., Lu, S.L., Zhang, M.X., Deng, C., and Wang, X.J. 2004. Smad3 knockout mice exhibit a resistance to skin chemical carcinogenesis. *Cancer Res.* **64**:7836–7845.
45. Wreesmann, V.B., Estilo, C., Eisele, D.W., Singh, B., and Wang, S.J. 2007. Downregulation of Fanconi anemia genes in sporadic head and neck squamous cell carcinoma. *ORL J. Otorhinolaryngol. Relat. Spec.* **69**:218–225.
46. Marsit, C.J., et al. 2004. Inactivation of the Fanconi anemia/BRCA pathway in lung and oral cancers: implications for treatment and survival. *Oncogene.* **23**:1000–1004.
47. Berton, T.R., et al. 2003. Tumor formation in mice with conditional inactivation of Brca1 in epithelial tissues. *Oncogene.* **22**:5415–5426.
48. Kanamoto, T., Hellman, U., Heldin, C.H., and Souchelnytskyi, S. 2002. Functional proteomics of transforming growth factor-beta1-stimulated Mv1Lu epithelial cells: Rad51 as a target of TGFbeta1-dependent regulation of DNA repair. *EMBO J.* **21**:1219–1230.
49. Dubrovska, A., et al. 2005. TGFbeta1/Smad3 counteracts BRCA1-dependent repair of DNA damage. *Oncogene.* **24**:2289–2297.
50. Chen, Z., et al. 1999. Expression of proinflammatory and proangiogenic cytokines in patients with head and neck cancer. *Clin. Cancer Res.* **5**:1369–1379.
51. Kim, B.G., et al. 2006. Smad4 signalling in T cells is required for suppression of gastrointestinal cancer. *Nature.* **441**:1015–1019.
52. Rosendahl, A., et al. 2002. Activation of bone morphogenetic protein/Smad signaling in bronchial epithelial cells during airway inflammation. *Am. J. Respir. Cell Mol. Biol.* **27**:160–169.
53. Bharathy, S., Xie, W., Yingling, J.M., and Reiss, M. 2008. Cancer-associated transforming growth factor beta type II receptor gene mutant causes activation of bone morphogenic protein-Smads and invasive phenotype. *Cancer Res.* **68**:1656–1666.
54. Liu, I.M., et al. 2009. TGFbeta-stimulated Smad1/5 phosphorylation requires the ALK5 L45 loop and mediates the pro-migratory TGFbeta switch. *EMBO J.* **28**:88–98.
55. Bornstein, S., Hoot, K., Han, G.W., Lu, S.L., and Wang, X.J. 2007. Distinct roles of individual Smads in skin carcinogenesis. *Mol. Carcinog.* **46**:660–664.
56. Tang, K.F., et al. 2001. A distinct expression of CC chemokines by macrophages in nasopharyngeal carcinoma: implication for the intense tumor infiltration by T lymphocytes and macrophages. *Hum. Pathol.* **32**:42–49.
57. Patel, B.P., Shah, S.V., Shukla, S.N., Shah, P.M., and Patel, P.S. 2007. Clinical significance of MMP-2 and MMP-9 in patients with oral cancer. *Head Neck.* **29**:564–572.
58. Kundu, J.K., and Surh, Y.J. 2008. Inflammation: gearing the journey to cancer. *Mutat. Res.* **659**:15–30.
59. Garcia-Higuera, I., et al. 2001. Interaction of the Fanconi anemia proteins and BRCA1 in a common pathway. *Mol. Cell.* **7**:249–262.
60. Ratnam, K., and Low, J.A. 2007. Current development of clinical inhibitors of poly(ADP-ribose) polymerase in oncology. *Clin. Cancer Res.* **13**:1383–1388.